Acta Cryst. (1993). B49, 787–794

Determination of the Two-Dimensional Incommensurately Modulated Structure of Mo_2S_3

BY W. J. SCHUTTE, F. DISSELBORG AND J. L. DE BOER

Materials Science Centre, Laboratory of Inorganic Chemistry, University of Groningen, Nijenborgh 16, 9747 AG Groningen, The Netherlands

(*Received* 24 *October* 1990; *accepted* 22 *June* 1992)

Abstract

The incommensurately modulated structure of molybdenum sesquisulfide Mo_2S_3, with modulation wavevectors $\mathbf{q}_1 = -0.056\,(1)\mathbf{a}^* + 0.500\,(1)\mathbf{b}^* + 0.229\,(1)\mathbf{c}^*$ and $\mathbf{q}_2 = \frac{1}{2}\mathbf{a}^* + 0.469\,(1)\mathbf{b}^*$ at room temperature, has been determined by X-ray diffraction. The lattice parameters of the primitive monoclinic cell are: $a = 6.0868\,(4)$, $b = 3.2046\,(1)$, $c = 8.6233\,(5)$ Å, $\beta = 102.443\,(6)^\circ$ [with $\alpha = 89.995\,(5)$ and $\gamma = 90.010\,(7)^\circ$], $V = 164.3$ Å^3, $Z = 2$, $\mu = 90.4$ cm^{-1} ($\lambda = 0.7107$ Å), $M_r = 288.1$. The symmetry of the structure can be described as consisting of two independent one-dimensional modulated systems each with a four-dimensional superspace group with the same subcell structure $P2_1/m$. The $\mathbf{q}_1$ system is described with $P^{P\bar{1}}_{\bar{1}}(\alpha\beta\gamma)$ and consists of two domains (related by m_y), and the $\mathbf{q}_2$ system is described with $A^{P2_1/m}_{\bar{1}\bar{1}}(\frac{1}{2}\beta 0)$. The final R factor is 0.063 for 10 264 reflections. Alternatively, the structure can be described with the triclinic five-dimensional superspace group $P^{P\bar{1}}_{P\bar{1}}(\alpha\beta\gamma)(\lambda\mu\nu)$ giving a final R_F factor of 0.061 for 13 164 reflections. In the modulated structure the two independent Mo zigzag chains are distorted towards different types of four- and three-metal-atom clustering, with the S atoms squeezed out so as to keep the Mo–S distances as for the undistorted case.

1. Introduction

The compound Mo_2S_3 has been studied by several authors (McCabe, 1955; Jellinek, 1961). Jellinek (1961) found the basic structure from X-ray powder data to be monoclinic, space group $P2_1/m$. The S atoms form close-packed layers with a *chh*-type stacking sequence along **b**. The octahedral sites between two *hh* stacked layers are all occupied [by Mo(1)], whereas only half of the octahedral sites between *ch* layers are filled [by Mo(2)] (see Fig. 1). As a result of metal-atom bonding (Mo–Mo bonding) the rhombohedral symmetry is destroyed and the structure becomes monoclinic. The Mo atoms are displaced in such a way that two types of infinite Mo zigzag chains are formed, both running along **b**. The compounds Nb_2Se_3 and Ta_2Se_3 are isotypic with Mo_2S_3 (Kadijk, Huisman & Jellinek, 1968).

From Weissenberg photographs (de Jonge, Popma, Wiegers & Jellinek, 1970) extra reflections were observed and it was concluded that the true structure is more complex. Deblieck *et al.* (1983) and Deblieck, van Landluyt, van Dyck, van Tendeloo & Amelinckx (1987) made attempts to unravel the complex structure of Mo_2S_3 by also taking into account the weak superstructure reflections. Two different incommensurate wavevectors were revealed and several lock-in transitions were observed. On heating, the $\mathbf{q}_2$ satellites vanish at a lower temperature than the $\mathbf{q}_1$ satellites. The structure of the commensurate phase at 100 K with $\mathbf{q}_1 = (0,\frac{1}{2},\frac{1}{4})$ and $\mathbf{q}_2 = (\frac{1}{2},\frac{1}{2},0)$ was determined using a supercell $a \times 2b \times 4c$ and $2a \times 2b \times c$, respectively. The true triclinic structure was related to the results of a monoclinic refinement and it was found that four-atom clusters are present in chains of both types. A combination of electron microscopy and X-ray diffraction was used to make a structure proposal for the phases involved in the different transitions. HREM results (Deblieck *et al.*,

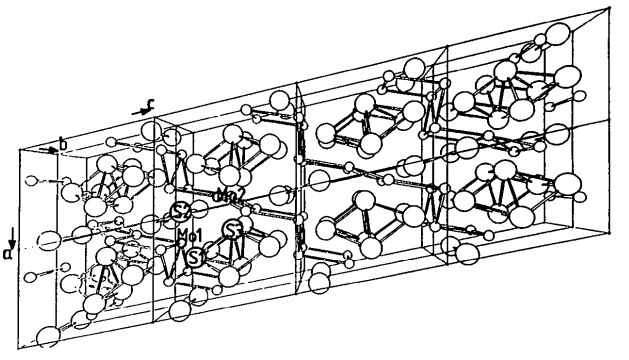

Fig. 1. Average monoclinic structure of Mo_2S_3 viewed along **b** ($2a \times 2b \times 4c$ unit cells). Small circles represent Mo atoms, the larger circles S atoms. The atom labelling is indicated. Bonding lines are given for $r_{S\text{–}S} < 3.3$ Å and $r_{Mo\text{–}Mo} < 3.3$ Å. The plane of the zigzag chain of Mo(1) is approximately parallel to [001], while the plane of the zigzag chain of Mo(2) is almost parallel to [$\bar{1}$01].

©1993 International Union of Crystallography
Printed in Great Britain – all rights reserved

1987) favoured a continuous deformation modulation rather than a modulation featuring sharp interfaces.

de Jonge *et al.* (1970) measured the electrical-transport and magnetic properties of single crystals of Mo_2S_3, which showed that the compound is metallic. Significant changes noticed at low temperature indicate several phase changes. Low-temperature X-ray diffraction showed a transition at about 193 K to a triclinic structure. Also at about 390 K a phase transition accompanied by disappearance of the superstructure reflections was found (Deblieck *et al.*, 1983). Another phase transition was reported by Rastogi (1985) at about 135 K with an unusual time dependence of the isothermal resistivity. Simultaneously with the phase transitions the physical properties changed. Nonequilibrium physical properties were measured by Fagerquist, Kirby & Pearlstein (1989) and explained in terms of a model with a double-well potential model for the charge carriers. Various physical models for the charge carriers in Mo_2S_3 were proposed to explain the measurements: a charge-density-wave (CDW) model (Hemmel, van der Heide, van Bruggen, Haas & Wiegers, 1983), an acoustical polaron model (Fagerquist *et al.*, 1989) and a band Jahn–Teller model (Rastogi, 1985). Significant differences in behaviour were found between different crystals. Deblieck *et al.* (1987) found that most crystals consisted of two orientation variants. Both variants – monodomain and polydomain single crystals – have different behaviour as a function of temperature below room temperature.

In this paper we give an X-ray structure refinement of the incommensurate room-temperature phase of Mo_2S_3 based on the superspace-group approach of Janner, Janssen & de Wolff (1983) and analyse and discuss the structural modulations. In doing so, we can describe the modulation of the structure, especially the clustering of the metal atoms, in considerably more detail than given in the analysis by Deblieck *et al.* (1987) of the incommensurate phase.

2. Experimental

Single crystals from the same batch as used by Deblieck *et al.* (1983) were taken. Molybdenum(III) sulfide crystals were grown by vapour transport (without an added foreign agent). In this batch, named $Mo_{2.065}S_3$ on the basis of chemical analysis, we found small single crystals of Mo metal. This indicates that excess Mo is present as a second phase; we have no reason to doubt the stoichiometric character of the compound, which we will name Mo_2S_3 hereafter. The results of the X-ray structure refinement also give no indications for deviations from the stoichiometry of Mo_2S_3. All diffraction experiments were performed with monochromatized Mo $K\alpha$ radiation on an Enraf–Nonius CAD-4F diffractometer equipped with a modified CAD-4 program (de Boer & Duisenberg, 1984). All observed reflections could be indexed as $hklm_1m_2$ with hkl the Miller indices corresponding to the monoclinic subcell and $|m_1|$, $|m_2|$ the orders of the satellite reflections of the two modulation wavevectors $\mathbf{q}_1$ and $\mathbf{q}_2$, respectively. We investigated both needle and platelet crystals but did not find any significant differences, either in cell dimensions or in modulation vectors $\mathbf{q}$, between them.

For the final measurements we selected a needle along $\mathbf{b}$ with dimensions of about $0.04 \times 0.6 \times 0.03$ mm. Lattice parameters were obtained from the positions of higher-order reflections. The modulation wavevectors $\mathbf{q}_1$ and $\mathbf{q}_2$ were determined from accurately determined positions of first-order satellites, giving $\mathbf{q}_1 = [-0.056\ (1), 0.500\ (1), 0.229\ (1)]$ and $\mathbf{q}_2 = [\frac{1}{2}, 0.469\ (1), 0]$. Intensity data were collected using the θ–2θ scan method for a hemisphere, up to $\theta = 50°$ for the main, $\mathbf{q}_1$ and $\mathbf{q}_2$ reflections. Only first-order satellites could be measured; sum satellites $\mathbf{q}_1 + \mathbf{q}_2$ and higher-order satellites were not observed.

The standard background procedure for calculating net intensities suffered serious problems for the $\mathbf{q}_2$ satellites due to the partial overlap of $h,k,l,m_1 = 0,m_2$ and $h + m_2,k + m_2,l,m_1 = 0, -m_2$ reflections; these reflections differ by only $0.062\mathbf{b}^*$ for $|m_2| = 1$. Therefore, the full profiles of the $\mathbf{q}_2$ satellites were measured, at a scan speed four times lower than for $\mathbf{q}_1$, the azimuth angle ψ being chosen such that a maximum separation of the neighbouring satellites was attained. In the analysis of these profile measurements the individual satellites could be well separated.

Throughout the measurement three intensity-control reflections were monitored every 2 h and used for slight drift corrections (within $\pm 1.5\%$). With these reflections included we obtained a datafile of 21 412 reflections (including additional measurements for main reflections and $\mathbf{q}_2$ satellites). Hereafter, the data were corrected for Lorentz and polarization effects, for the volume of the crystal outside the beam ($d_\perp = 0.5$, $d_\parallel = 0.7$ mm) and for absorption (with absorption coefficient $\mu = 90.4\ \text{cm}^{-1}$; transmission factors 0.77–0.16). Unique data sets were subsequently obtained by averaging equivalent reflections; for details see Table 1.

3. Symmetry and refinement

The symmetry of the main reflections is $P2_1/m$, in accordance with the results of Jellinek (1961). The $\mathbf{q}_2$ satellites with modulation wavevector $\mathbf{q}_2 = \frac{1}{2}\mathbf{a}^* + 0.469\mathbf{b}^*$ fulfil the monoclinic symmetry, while the $\mathbf{q}_1$ satellites are clearly triclinic, as can be seen from

Table 1. *Total number of reflections, number of inequivalent reflections, number of inequivalent reflections with $I > 2.5\sigma(I)$ and the internal consistency, R_I*

The statistical accuracy in the measurements of the series for $\mathbf{q}_1$ and $\mathbf{q}_2$ satellites was roughly equal. For the main reflections and the $\mathbf{q}_2$ satellites, additional measurements were made and they were used in the averaging process. In this way values for R_I in the triclinic symmetry were also obtained.

$$R_I = \sum_j \{N_j \sum_i [(\langle I\rangle_j - \langle I\rangle_{i,j})^2/\sigma^2_{I,i,j}]\}^{1/2} / \sum_j [(N_j - 1)\sum_i I^2_{i,j}/\sigma^2_{I,i,j}]^{1/2}$$

with $\sum_j$ = summation over all independent reflections and $\sum_i$ = summation over all N_j symmetrically equivalent reflections for unique reflection j.

	Measured	Unique	With $I > 2.5\sigma(I)$	R_I
Monoclinic symmetry				
Main reflections	5799	1901	1758	0.024
First-order $\mathbf{q}_1$ reflections	6885	3459	3203	0.242
First-order $\mathbf{q}_2$ reflections	8725	3289	2676	0.060
All reflections	21409	8649	7637	
Triclinic symmetry				
Main reflections	5802	3423	3063	0.016
First-order $\mathbf{q}_1$ reflections	6885	6885	5830	
First-order $\mathbf{q}_2$ reflections	8725	5687	4271	0.052
All reflections	21412	15995	13164	

column R_I in Table 1 (also checked by measuring selected independent reflections). So the diffraction symmetry of both main and satellite reflections as a whole is $P\bar{1}$, leading in superspace to the (3 + 2)-dimensional Bravais class $P\bar{1}(\alpha\beta\gamma)(\lambda\mu\nu)$ (Janner, Janssen & de Wolff, 1983). A (3 + 2)-dimensional superspace group is given by the group of operators $(\mathfrak{R},\varepsilon|\tau)$, where $\mathfrak{R}$ represents the point group on the three-dimensional part and ε transforms the two-dimensional internal space. $\boldsymbol{\tau} = (\tau_x,\tau_y,\tau_z,\tau_4,\tau_5)$ is the five-dimensional translational part of the operator. $P\bar{1}(\alpha\beta\gamma)(\lambda\mu\nu)(p2)$ is the corresponding centrosymmetric superspace group, which has the equivalent positions (taking $\bar{1}$ at the origin)

$$(x,y,z,x_4,x_5),\ (-x,-y,-z,-x_4,-x_5). \qquad (1)$$

The five-dimensional triclinic superspace symmetry for the structure as a whole (called the full triclinic description) can be reduced to two subsystems (called the partially monoclinic description): the systems $\mathbf{q}_1$ and $\mathbf{q}_2$. This reduction into two one-dimensional modulation systems is possible because sum satellites of the form $\mathbf{q}_1 + \mathbf{q}_2$ could not be observed. Even in an electron diffraction study, Deblieck *et al.* (1987) concluded that these sum satellites were absent. Thus two independent one-dimensional modulated systems exist with negligible coupling between them. The subcell structure and the $\mathbf{q}_2$ system exhibit monoclinic symmetry. Evidently, the triclinic modulation $\mathbf{q}_1$ does not seriously affect the symmetry of the monoclinic subcell structure and the $\mathbf{q}_2$ distortion. We give a symmetry description in this (3 + 1 + 1)-dimensional superspace in which the monoclinic symmetry for the average structure and for the $\mathbf{q}_2$ system is maintained.

Table 2. *Symmetry restrictions on the components of the modulation function for the monoclinic superspace group*

It is indicated whether a particular component is even or odd.

Atom	Component	Symmetry
All	u_x, u_z	Odd
	u_y	Even

For the $\mathbf{q}_1$ system we have the Bravais class $P\bar{1}(\alpha\beta\gamma)$, giving the centrosymmetric superspace group $P\bar{1}(\alpha\beta\gamma)(\bar{1})$ and the equivalent positions

$$(x,y,z,x_4),\ (-x,-y,-z,-x_4). \qquad (2)$$

For the $\mathbf{q}_2$ system we have the four-dimensional Bravais class $P2/m(\frac{1}{2}\beta 0)$ and from the extinction $k = 2n$ for $0k00$ reflections the centrosymmetric superspace group is $P2_1/m(\frac{1}{2}\beta 0)(1\bar{1})$. We transform the subcell so that only the irrational component in $\mathbf{q}_2$ remains. The a axis is thereby doubled and two different screw axes (2_1, 2_1) exist. To be in accordance with the atomic coordinates of de Jonge *et al.* (1970), we take ($\frac{2_1/m}{1}$) at the origin. The resulting equivalent positions are

$$(x,y,z,x_5),\ (x+\tfrac{1}{2},y,z,x_5+\tfrac{1}{2}) +$$
$$(-x,-y,-z,-x_5),\ (-x,y+\tfrac{1}{2},-z,x_5+\tfrac{1}{2}),$$
$$(x,-y+\tfrac{1}{2},-z,-x_5+\tfrac{1}{2}). \qquad (3)$$

We will consider a displacive modulation function for each atom μ. The modulation is a periodic function of $\bar{x}^\mu_4 = \mathbf{q}_1.\mathbf{r}^\mu_0$ and $\bar{x}^\mu_5 = \mathbf{q}_2.\mathbf{r}^\mu_0$, and is defined by the atomic displacements of $\mathbf{u}^\mu = \mathbf{r}^\mu - \mathbf{r}^\mu_0$ from their average position $\mathbf{r}^\mu_0$. The x,y,z components of these displacements $\mathbf{u}^\mu$ are given by

$$u^\mu_i(\bar{x}^\mu_4,\bar{x}^\mu_5) = \sum_{j=1}^{M}\sum_{n=1}^{N} u^{\mu;j,c}_{n,i}\cos(2\pi n\bar{x}^\mu_{3+j}) + u^{\mu;j,s}_{n,i}\sin(2\pi n\bar{x}^\mu_{3+j}),\quad i = x,y,z, \qquad (4)$$

with $u^{\mu;j}_{n,i}$ the nth harmonic Fourier amplitude of the modulation wave for the jth independent modulation wavevector and $M = 2$, $N = 1$, since we observed two independent modulation wavevectors and only first-order satellite reflections.

In the triclinic space group all atoms occupy general positions, but in the monoclinic superspace group all atoms lie on the mirror plane and modulation parameters are restricted (Table 2). We see that in this superspace group all allowed modulation functions are either even or odd.

The least-squares program *REMOS*85 (Yamamoto, 1985), which calculates the structure factors in

the higher-dimensional analysis, has been used for the refinement. Refinement of the variables, with one extra parameter describing the secondary extinction, was performed by minimizing R_F. The definition of the R factors is

$$R_F = \sum w||F_{obs}| - |F_{calc}||/\sum w|F_{obs}| \quad (5)$$

and

$$R_{F^2} = [\sum(w|F_{obs}| - |F_{calc}|)^2/\sum w|F_{obs}|^2]^{1/2}. \quad (6)$$

The atomic scattering factors and the anomalous-dispersion factors were taken from the *International Tables for X-ray Crystallography* (1974, Vol. IV). We started our calculation with the results of de Jonge *et al.* (1970) for the average structure: Mo(1) at (0.310, $\frac{1}{4}$, 0.009), Mo(2) at (0.108, $\frac{1}{4}$, 0.632), S(1) at (0.505, $\frac{1}{4}$, 0.803), S(2) at (0.963, $\frac{1}{4}$, 0.161) and S(3) at (0.729, $\frac{1}{4}$, 0.516). Next all possible displacive waves were included. For all reflections with $I > 2.5\sigma$, unit weight is taken, and, for those with $I < 2.5\sigma$, zero weight is taken.

Structural refinements for the $\mathbf{q}_1$ part of the structure in the partially constrained monoclinic and triclinic descriptions were not successful if a single-domain structure is assumed ($R_F = 0.291$). The refinement succeeded by considering the triclinic structure to consist of two domains, related to each other by the mirror plane m_y. Of course, such twinning does not affect the monoclinic parts of the structure (main reflections and $\mathbf{q}_2$ system) but it does affect the triclinic $\mathbf{q}_1$ system, where now, because $q_{1,y} = \frac{1}{2}$ within the standard deviation, reflections $h,k,l,m_1,m_2 = 0$ of domain I and reflections $h,-k-m_1,l,m_1,m_2 = 0$ of domain II coincide. The relative volumes of the two domains become an extra refinement parameter. The final refinement results are listed in Table 3 (R factors) and Table 4 (positional parameters for the partially monoclinic refinement). The corresponding temperature parameters are listed in Table 5. The relative volumes of the two domains are 58:42 for partially monoclinic structure refinement and 55:45 for the fully triclinic refinement.

Table 3. *R_F and R_{F^2} values of the refinement for the final results*

The number of parameters (n_p) and the number of reflections (n_r) used are also given in the table.

	R_F	R_{F^2}	n_p	n_r
Partially monoclinic				
Main	0.029	0.031	32	1758
$\mathbf{q}_1$	0.083	0.097	31	5830
$\mathbf{q}_2$	0.098	0.115	15	2676
Overall	0.065	0.053	78	10264
Fully triclinic				
Main	0.031	0.034	47	3063
$\mathbf{q}_1$	0.086	0.100	31	5830
$\mathbf{q}_2$	0.090	0.105	30	4271
Overall	0.061	0.055	108	13164

Table 4. *Final values for the coordinates and amplitudes of the modulation functions*

All coordinates are with respect to the doubled ($2a$) unit cell, with modulation wavevectors being transformed to $\mathbf{q}_1 = (-0.112, 0.500, 0.229)$ and $\mathbf{q}_2 = (0, 0.469, 0)$, and with $\mathbf{x}_0^\mu$ as the average position in this basic unit cell.

μ,i	$x^\mu_{0,i}$	$u^{\mu,1,c}_{i,i}$	$u^{\mu,1,s}_{i,i}$	$u^{\mu,2,c}_{i,i}$	$u^{\mu,2,s}_{i,i}$
Mo(1)					
x	0.15482 (1)	−0.00023 (4)	−0.00011 (4)		−0.00351 (3)
y	$\frac{1}{4}$	−0.0022 (2)	0.0112 (2)	0.0484 (1)	
z	0.00924 (2)	−0.00177 (6)	0.00225 (6)		−0.00005 (4)
Mo(2)					
x	0.05454 (2)	0.00231 (4)	−0.00046 (5)		−0.00138 (3)
y	$\frac{1}{4}$	0.0155 (7)	−0.0534 (2)	0.0015 (1)	
z	0.63058 (2)	0.00340 (5)	−0.00053 (7)		−0.00077 (4)
S(1)					
x	0.25522 (5)	0.0013 (1)	−0.0016 (1)		−0.00740 (8)
y	$\frac{1}{4}$	0.0052 (4)	−0.0083 (4)	0.0077 (2)	
z	0.80350 (6)	0.0019 (2)	0.0010 (2)		−0.0063 (1)
S(2)					
x	0.48603 (4)	0.0006 (1)	−0.0012 (1)		0.00441 (7)
y	$\frac{1}{4}$	−0.0005 (4)	0.0074 (3)	−0.0099 (2)	
z	0.15656 (6)	−0.0021 (1)	0.0003 (1)		0.0036 (1)
S(3)					
x	0.36411 (5)	0.0005 (1)	−0.0004 (1)		0.00167 (8)
y	$\frac{1}{4}$	0.0021 (4)	−0.0048 (4)	0.0017 (3)	
z	0.51374 (8)	0.0147 (2)	−0.0005 (3)		0.0023 (1)

Table 5. *Temperature parameters*

The anisotropic thermal parameter is given by $\exp[-(\beta_{11}h^2 + \beta_{22}k^2 + \beta_{33}l^2 + 2\beta_{13}hl)]$. The β_{ij} are with respect to the halved ($\frac{1}{2}\mathbf{a}^*$) reciprocal unit cell.

	Mo(1)	Mo(2)	S(1)	S(2)	S(3)
β_{11}	0.000543 (7)	0.000679 (7)	0.00091 (2)	0.00074 (2)	0.00074 (2)
β_{22}	0.0089 (1)	0.0082 (1)	0.0085 (3)	0.0091 (3)	0.0095 (3)
β_{33}	0.00115 (1)	0.00134 (2)	0.00134 (4)	0.00166 (4)	0.00262 (7)
β_{13}	0.000149 (7)	0.000176 (7)	0.00019 (2)	0.00032 (2)	0.00030 (3)

4. Discussion

The average structure of monoclinic Mo_2S_3 (Fig. 1) is basically equivalent with the structure as determined by de Jonge *et al.* (1970), with the same short Mo–Mo chains (see Table 6).

In the modulated structure the zigzag chains of Mo atoms become distorted. Fig. 2 shows the displacements in the $\mathbf{q}_1$ and $\mathbf{q}_2$ systems. The strongest distortions on the Mo(1) and Mo(2) atoms are along $\mathbf{b}$ and come from the $\mathbf{q}_2$ and $\mathbf{q}_1$ systems, respectively. We see that in the zigzag chains coupled four-atom clusters of Mo are present, which were also observed at 100 K (Deblieck *et al.*, 1983).

In the $\mathbf{q}_2$ system in addition to four-atom clusters there exist regions with three-atom clusters (Fig. 2*b*). At phases of the modulation wave $\bar{x}_5^\mu = (2n+1)/8$ the Mo displacements in the chain have equal values for the atoms on the left and right-hand sides of the chain, forming four-atom clusters. However, further

Table 6. *Interatomic distances* (Å) *and bond strengths s in the average structure of* Mo_2S_3

	Coordination	Distance	s		Coordination	Distance	s
Mo(1)	2 × S(1)	2.36	0.61	Mo(2)	2 × S(3)	2.37	0.59
	1 × S(1)	2.37	0.59		1 × S(3)	2.32	0.67
	2 × S(2)	2.55	0.39		2 × S(1)	2.56	0.38
	1 × S(2)	2.64	0.32		1 × S(1)	2.57	0.37
	Average	2.47			Average	2.46	
	Σs		2.92		Σs		2.98
	2 × Mo(1)	2.85	1.21		2 × Mo(2)	2.85	1.21
	2 × Mo(1)	3.20	0.32		2 × Mo(2)	3.20	0.32
	1 × Mo(2)	3.23	0.28		1 × Mo(1)	3.23	0.28
	2 × Mo(1)	4.07	0.01				
	Σs		3.36		Σs		3.35

	Coordination	Distance		Coordination	Distance		Coordination	Distance
S(1)	1 × S(3)	3.07	S(2)	2 × S(2)	3.20	S(3)	1 × S(1)	3.07
	2 × S(1)	3.20		2 × S(2)	3.22		2 × S(3)	3.17
	2 × S(3)	3.23		2 × S(1)	3.42		2 × S(3)	3.20
	2 × S(2)	3.42		2 × S(3)	3.42		2 × S(1)	3.23
	2 × S(2)	3.49		2 × S(1)	3.49		2 × S(2)	3.42
	1 × S(1)	3.67		1 × S(1)	3.67		1 × S(2)	3.69
	2 × S(1)	3.78		1 × S(3)	3.69		2 × S(3)	3.73

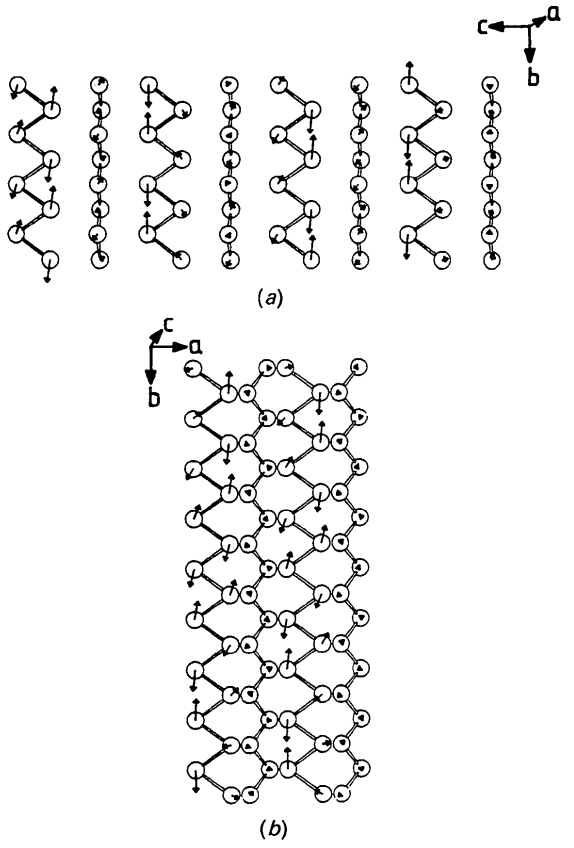

Fig. 2. Modulation displacements in Mo–Mo zigzag chains: (*a*) viewed along the *a* axis ($4c \times 4b$), leftmost chain is one of Mo(2); (*b*) viewed along the *c* axis ($2a \times 9b$), leftmost chain is one of Mo(1). Displacements for the Mo atoms are represented, in direction and in length (exaggerated by a factor of 8) by the arrows. In (*a*) the distortion associated with the $\mathbf{q}_1$ modulation is given; in (*b*) the distortion is shown for the $\mathbf{q}_2$ modulation.

down the *b* axis, at $\bar{x}_5^{\mu} = 2n/8$, the displacements of the Mo atoms have a larger value on one side of the chain [a pseudo-mirror-plane antiphase boundary (APB) is located here], forming three-atom clusters. Along the **b** direction the displacements of the Mo atoms gradually change from one type with four-atom clusters to another type with three-atom clusters with a period of about eight unit cells. Neighbouring chains along **a** are in antiphase.

For the $\mathbf{q}_1$ system we also have a distortion of the Mo chain with the formation of three- and four-atom clusters. However, neighbouring Mo chains are not in antiphase as for the $\mathbf{q}_2$ system but are incommensurable in the *ac* plane (see Fig. 2*a*). Because of the commensurable component q_{1y} only one type of cluster is present in each Mo(2) chain. Therefore, an important difference in the type of clustering between the two subsystems exists; in the $\mathbf{q}_1$ system only one type of clustering is present in a chain and different cluster types occur in other chains, while in the $\mathbf{q}_2$ system all cluster types occur within each chain, with no differences between the chains. The reason for twinning in the triclinic $\mathbf{q}_1$ system is now obvious because the distortion of the monoclinic subcell towards one type of cluster (domain I) is equally as probable as the distortion towards clusters with the mirror (m_y) image (domain II).

In Fig. 3 we see that the S atoms displace mainly as a result of the Mo clustering. The S atoms, S(3) being the nearest neighbour of Mo(2) in the $\mathbf{q}_1$ system and S(1), S(2) being nearest neighbours of Mo(1) in the $\mathbf{q}_2$ system, move in the direction of the free space created by the Mo clustering; thus the S atoms are squeezed out of the metal clusters.

The anisotropic temperature factors in the incommensurable structure for all atoms deviate only slightly from isotropic; even the difference in the temperature factors between the independent atoms is very small. The structure can thus be represented as a close packing of sulfur spheres without strongly anisotropic interactions.

Interatomic distances from both Mo(1) and Mo(2) to the surrounding atoms were calculated (deposited as Figs. 4 and 5*) for the $\mathbf{q}_1$ and $\mathbf{q}_2$ deformations, respectively, as a function of the phase parameters $\varphi_1 = \bar{x}_4^{\mu} - \mathbf{q}_1.\mathbf{x}_0 \pmod 1$ and $\varphi_2 = \bar{x}_5^{\mu} - \mathbf{q}_2.\mathbf{x}_0 \pmod 1$. The Mo–S distances do not show strong deviations from their average values. The average octahedral distortion ($\Delta_{oct} = 0.30$ Å) is larger than the modulation displacements ($\Delta_{mod} = 0.15$ Å). The modulation in the Mo–Mo distances is much larger ($\Delta_{mod} =$

* Lists of structure factors and figures showing the Mo coordination in the $\mathbf{q}_1$ and $\mathbf{q}_2$ systems have been deposited with the British Library Document Supply Centre as Supplementary Publication No. SUP 71023 (80 pp.). Copies may be obtained through The Technical Editor, International Union of Crystallography, 5 Abbey Square, Chester CH1 2HU, England.

0.80 Å). The shortest Mo–Mo distance is 2.73 Å in the $\mathbf{q}_1$ and 2.79 Å in the $\mathbf{q}_2$ system and nearly equal to the metal–metal distance in the pure element: Mo–Mo = 2.73 Å. Each Mo atom is involved in the formation of intermetallic bonds, with the number of bonds varying between 2 and 3, depending on the phase of the modulation wave.

The distance between a pair of bonded atoms is a function of the strength of the bond between these atoms (Pauling, 1960; Brown & Shannon, 1973). A more quantitative estimate of the relative strength of the Mo–S and Mo–Mo bonds and the distribution of the 4*d* electrons can be obtained by empirical correlations, which have been tabulated for many types of bonds. With Pauling's (1960) valence sum rule, values for the atomic valencies ($\sum s$) can be found. For the Mo–S bond strength we use the relation

$$s = (r/r_0)^{-N} \tag{7}$$

with $r_0 = 2.167$ Å and N = 5.8 (Brown, 1981). For the Mo–Mo metallic bond we use the relation

$$r = r_0 - 0.60 \log s \tag{8}$$

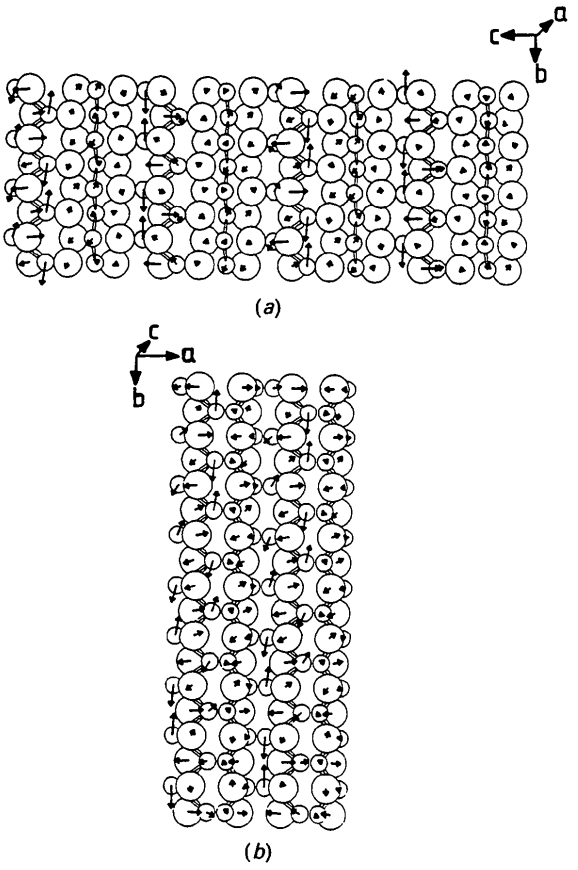

Fig. 3. (*a*), (*b*) Same as Fig. 2 but now, besides Mo atoms, their closest neighbouring S atoms (larger circles) with their displacements are also given.

proposed by Pauling (1960). We take $r_0 = 2.90$ Å [single bond length between Mo–Mo atoms from Slater (1964)] for a bond of unit strength in the Mo zigzag chain. In Table 6 we have given the bond strengths for the average structure. The valencies for the Mo atoms are in close agreement with the expected value of 3, corresponding to three 4*d* electrons per Mo atom. The small difference between the valencies of Mo(1) and Mo(2) could indicate a slightly larger number of *d* electrons on the atoms in the Mo(1) chain. We can also derive the atomic valencies for the real structure (including the modulation displacements). It is found that the valencies of Mo atoms in a cluster are higher. Thus the cluster formation corresponds to a pile-up of Mo 4*d* electrons in clusters. The three *d* electrons on the Mo^{3+} ion would in the undeformed lattice be delocalized over the infinite zigzag chains; in the real structure these electrons are delocalized over the atoms of a cluster. Moreover, we conclude that the manner of electron pile-up in metal clusters in the $\mathbf{q}_2$ system is the same for all chains, while in the $\mathbf{q}_1$ system it differs for different chains.

The valencies of the Mo(1) and Mo(2) atoms for the $\mathbf{q}_2$ and $\mathbf{q}_1$ modulation, respectively, are modulated along the chain direction, pointing to a commensurate and an incommensurate CDW. For the metallic valence in the average structure we find that 3.35 electrons per Mo atom are involved in Mo–Mo bonds. Thus more electrons (about 0.30 electrons per Mo atom) are found to be present in Mo–Mo bonds than are available on the basis of a completely filled anion valence band. Then there must be about 0.30 holes per Mo atom present in the valence band. As we observe interatomic S–S distances of 3.07 Å, being between the $(S^{2-})_2$ (3.50 Å) and the $(S_2)^{2-}$ (2.05 Å) interatomic distances, we expect that these holes in the valence band are partly removed by the creation of S–S bonding. This agrees with the transport properties measured by Hemmel *et al.* (1983), who supposed the presence of both electrons and hole carriers. They always found *p*-type behaviour for R_h with 0.103 holes per Mo atom at 298 K, decreasing at lower temperature. By the modulation at room temperature, leading to clustering (and probably also in the other clustering types at lower temperature), a different number of electrons get involved in the metal bonding (also a different number of holes become present), giving a different number of charge carriers along the chain direction.

The tendency of transition metals in transition-metal chalcogenides to form clusters is well known. Distorted structures with triangles of metal atoms have been observed for NbS (Kadijk & Jellinek, 1969). Four-atom clustering of metal atoms is often observed in d^3 transition-metal compounds and

resembles the modulations in Mo_2S_3. For instance, in $ReSe_2$, which has a different packing of the chalcogen atoms, all metal atoms are involved in zigzag chains and have undergone four-atom clustering. The large triclinic $ReSe_2$ cell (Alcock & Kjekshus, 1965) can be transformed ($a = 2A + \frac{1}{2}B$, $b = \frac{1}{2}B$, $c = \frac{1}{2}B + C$) to a smaller monoclinic basic cell with a triclinic distortion $\mathbf{q} = (\frac{1}{2},\frac{1}{2},\frac{1}{2})$, similar to the $\mathbf{q}_1$ distortion in Mo_2S_3. Other examples are $CoMo_2S_4$ and $FeMo_2S_4$ (Guillevic, Le Marouille & Grandjean 1974), also with four-atom clusters. The large noncentrosymmetric unit cell of $CoMo_2S_4$ can be transformed ($a = \frac{1}{2}A$, $b = \frac{1}{2}B$, $c = -A - C$) to a smaller centrosymmetric cell with a modulation $\mathbf{q} = (\frac{1}{2},\frac{1}{2},0)$, similar to the $\mathbf{q}_2$ distortion in Mo_2S_3. A final example with four-atom clustering is seen in the structures of Tc_2As_3 and Tc_2P_3 (Dietrich & Jeitschko, 1986; Jeitschko & Dietrich, 1985). Here the triclinic unit cell can be transformed ($a = -\frac{1}{2}A + 2B$, $b = \frac{1}{2}A$, $c = \frac{1}{2}A - B - C$) to the same monoclinic subcell as that of $ReSe_2$, with a triclinic distortion $\mathbf{q} = (\frac{1}{2},\frac{1}{2},\frac{1}{2})$. Both compounds with the $\mathbf{q}_1$-type distortion ($ReSe_2$, Tc_2P_3) are twinned as in Mo_2S_3, with their subcell still monoclinic to a very good approximation. An example with an extra occupation modulation besides displacive modulations is seen in the structure of the V_7S_8 phase (De Vries, 1972), with type I corresponding with $\mathbf{q}_2$ and type II probably with the $\mathbf{q}_1$ modulation of Mo_2S_3. The basic structure of V_7S_8 is that of V_3S_4 (isostructural with the average structure of $CoMo_2S_4$), with an extra site present (vacant in V_3S_4) that is occupationally modulated. A more detailed study of these commensurate modulations and the relation with the modulation in Mo_2S_3 will be discussed in a forthcoming paper.

The frequently observed antiphase ordering of neighbouring chains in transition-metal chalcogenides, which is also seen in the $\mathbf{q}_2$ system of Mo_2S_3, is not present in the $\mathbf{q}_1$ system. We can understand this because the distance between the neighbouring Mo(2) zigzag chains (with the strong $\mathbf{q}_1$ distortion) is much larger than the distance between neighbouring Mo(1) zigzag chains, leading to a more one-dimensional character for $\mathbf{q}_1$, without coupling between Mo(2) chains (*cf.* $NbSe_3$).

5. Concluding remarks

We have determined the Mo-cluster formation in the incommensurable room-temperature phase of Mo_2S_3. From the refinement we deduced that all atomic positions are fully occupied, giving the stoichiometric phase Mo_2S_3. The structure distorts to form clusters with metal–metal bonds. Several types of clustering exist in different chains for the $\mathbf{q}_1$ system and in the same chain for the $\mathbf{q}_2$ system. Large metallic valencies are found on the metal atoms in the clusters, giving a pile-up of 4*d* electrons in the clusters.

Structural distortions (incommensurate or commensurate with the basic structure) have been observed in many group V, VI and VII transition-metal chalcogenides as MX_4, MX_3, MX_2, $MX_{1.5}$, MX, where the metal atoms have d^1, d^2, d^3 configuration and are coordinated by the chalcogenide X (S, Se, Te) (Hulliger, 1976). Important parameters for the type of distortion are the type of packing, the possibility of pair formation and the polarizability of the anions and also the metal–metal interaction (number and delocalization of *d* electrons). In the incommensurate phase of Mo_2S_3 the distortion is now known in considerable detail and a further interpretation of the different types of clustering will be of interest.

This work is part of the research program of the Netherlands Foundation for Chemical Research (SON) and was made possible by financial support from the Netherlands Organisation for Scientific Research (NWO).

References

ALCOCK, N. W. & KJEKSHUS, A. (1965). *Acta Chem. Scand.* **19**, 79–94.

BOER, J. L. DE & DUISENBERG, A. J. M. (1984). *Enraf–Nonius CAD-4F Diffractometer Software Update, February* 1984. Enraf–Nonius, Groningen and Utrecht, The Netherlands.

BROWN, I. D. (1981). *Structure and Bonding in Crystals*, II, edited by M. O'KEEFFE & A. NAVROTSKY, pp. 1–30. New York: Academic Press.

BROWN, I. D. & SHANNON, R. D. (1973). *Acta Cryst.* A**29**, 266–282.

DEBLIECK, R., VAN LANDLUYT, J., VAN DYCK, D., VAN TENDELOO, G. & AMELINCKX, S. (1987). *J. Solid State Chem.* **70**, 108–120.

DEBLIECK, R., WIEGERS, G. A., BRONSEMA, K., VAN DYCK, D., VAN TENDELOO, G., VAN LANDLUYT, J. & AMELINCKX, S. (1983). *Phys. Status Solidi A*, **77**, 249–261.

DE VRIES, A. B. (1972). PhD thesis, Univ. of Groningen, The Netherlands.

DIETRICH, L. H. & JEITSCHKO, W. (1986). *J. Solid State Chem.* **63**, 377–385.

FAGERQUIST, R. L., KIRBY, R. D. & PEARLSTEIN, E. A. (1989). *Phys. Rev. B*, **39**, 5139–5151.

GUILLEVIC, J., LE MAROUILLE, J.-Y. & GRANDJEAN, D. (1974). *Acta Cryst.* B**30**, 111–117.

HEMMEL, R., VAN DER HEIDE, H., VAN BRUGGEN, C. F., HAAS, C. & WIEGERS, G. A. (1983). *Studies in Inorganic Chemistry*, edited by R. METSELAAR, H. J. M. HEYLIGERS & J. SCHOONMAN, pp. 691–694. Amsterdam: Elsevier Scientific.

HULLIGER, F. (1976). *Structural Chemistry of Layer-Type Phases*, edited by F. LEVY, pp. 21–50. Dordrecht: Reidel.

JANNER, A., JANSSEN, T. & DE WOLFF, P. M. (1983). *Acta Cryst.* A**39**, 671–678.

JEITSCHKO, W. & DIETRICH, L. H. (1985). *J. Solid State Chem.* **57**, 59–67.

JELLINEK, F. (1961). *Nature (London)*, **192**, 1065–1066.
JONGE, R. DE, POPMA, T. J. A., WIEGERS, G. A. & JELLINEK, F. (1970). *J. Solid State Chem.* **2**, 188–192.
KADIJK, F., HUISMAN, R. & JELLINEK, F. (1968). *Acta Cryst.* B**24**, 1102–1109.
KADIJK, F. & JELLINEK, F. (1969). *J. Less-Common Met.* **19**, 421–430.
MCCABE, C. L. (1955). *J. Met.* **7**, 61.
PAULING, L. (1960). *The Nature of the Chemical Bond.* Ithaca: Cornell Univ. Press.
RASTOGI, A. K. (1985). *Philos. Mag. B*, **192**, 909–919.
SLATER, J. C. (1964). *J. Chem. Phys.* **41**, 3199–3204.
YAMAMOTO, A. (1985). *REMOS*85.0. *Computer Program for the Refinement of Modulated Structures.* National Institute for Research in Inorganic Materials, Sakura-Mura, Niihari-Gun, Ibaraki 305, Japan.

Acta Cryst. (1993). B**49**, 794–806

X–N Study of the Electron Density in $(ND_4)_2Cu(SO_4)_2.6D_2O$ at 9 K: Flexible Radial Functions are Vital

BY BRIAN N. FIGGIS

Department of Chemistry, University of Western Australia, Nedlands, WA 6009, *Australia*

BO B. IVERSEN AND FINN K. LARSEN

Department of Chemistry, Aarhus University, DK 8000, *Aarhus C, Denmark*

AND PHILIP A. REYNOLDS

Department of Chemistry, University of Western Australia, Nedlands, WA 6009, *Australia*

(*Received* 4 *December* 1992; *accepted* 17 *March* 1993)

Abstract

Diammonium hexaaquacopper(II) disulfate-d_{20}, $[ND_4]_2[Cu(D_2O)_6](SO_4)_2$, $M_r = 419.7$, monoclinic $P2_1/a$, $a = 9.393$ (2), $b = 12.666$ (2), $c = 6.061$ (1) Å, $\beta = 107.16$ (1)°, $V = 689.0$ (4) Å^3, $Z = 2$, Mo $K\alpha$ radiation, $\lambda = 0.71069$ Å, $\mu = 2.01$ mm^{-1}, $F(000) = 415.3$ (414.0 without anomalous dispersion), $T = 9$ (1) K, $R(I) = 0.013$, $R(F) = 0.0095$, $\chi^2 = 0.89$, 5134 reflections. Refinement of the X-ray data, using a radially augmented multipolar charge model, gave thermal and positional parameters agreeing with those derived from neutron diffraction data and the correct cell content of electrons. The mean diagonal thermal-parameter difference between X-ray and neutron results is only 0.0003 Å^2. Two factors are vital in obtaining satisfactory and consistent fits to both experiments. (1) The use of a very low (< 10 K) temperature to eliminate thermal diffuse scattering and anharmonic effects, which are important even at 85 K. (2) The use of an electron-density model which includes more than one component in the atom-centred radial distributions; a single parameter 'κ' refinement is *not* adequate. The charge-density model is consistent with that obtained previously at 85 K, but is more precise, and uncertainties from possible systematic errors are much reduced. A simple valence model of the charge density, while still a good approximation, is no longer adequate. The reduced thermal motion at 9 K and use of neutron data reveal radial and angular density features which were not seen at 85 K, and which are inconsistent with simple valence models. However, they agree well with high-quality *ab initio* theoretical calculations. In particular, deep holes near the O and S nuclei are present in the theoretical maps, and are also significant in the experimental maps.

Introduction

The diammonium hexaaquametal(II) disulfates, examples of the Tutton salts, are excellent subjects for the study of metal–water bonding, and also of hydrogen bonding. The current state of our X-ray and polarized neutron diffraction (PND) studies of these systems, and other relevant experiments, have been summarized by Figgis, Khor, Kucharski & Reynolds (1992). That paper presented an X-ray diffraction study of the copper member of this series at 85 K. It showed the Jahn–Teller distortion of the copper 3*d* shell and both σ and π charge flow from the sulfate ion through water molecules to the Cu atom. The metal–water bonding found agreed quite well with theoretical calculations (Chandler, Christos, Figgis & Reynolds, 1992), but expected features such as lone pairs were not well resolved. In addition, substantial anharmonicity, connected with

©1993 International Union of Crystallography
Printed in Great Britain – all rights reserved